

## Title

A data-centric deep learning approach to airway segmentation

Wing Keung Cheung<sup>1,2</sup>, Ashkan Pakzad<sup>1,3</sup>, Nesrin Mogulkoc<sup>4</sup>, Sarah Needleman<sup>1,3</sup>, Bojidar Rangelov<sup>1,3</sup>, Eyjolfur Gudmundsson<sup>1,2</sup>, An Zhao<sup>1,2</sup>, Mariam Abbas<sup>2</sup>, Davina McLaverty<sup>5</sup>, Dimitrios Asimakopoulos<sup>6</sup>, Robert Chapman<sup>7</sup>, Recep Savas<sup>8</sup>, Sam M Janes<sup>9,10</sup>, Yipeng Hu<sup>1,3</sup>, Daniel C. Alexander<sup>1,2</sup>, John R Hurst<sup>10,11</sup>, Joseph Jacob<sup>1,9,10</sup>

<sup>1</sup>Satsuma Lab, Centre for Medical Image Computing, University College London, London, UK

<sup>2</sup>Department of Computer Science, University College London, London, UK

<sup>3</sup>Department of Medical Physics and Biomedical Engineering, University College London, London, UK

<sup>4</sup>Department of Respiratory Medicine, Ege University Hospital, Izmir, Turkey

<sup>5</sup>Medical School, University College London, London, UK

<sup>6</sup>School of Clinical Medicine, University of Cambridge, Cambridge, UK

<sup>7</sup>Interstitial Lung Disease Service, Department of Respiratory Medicine, University College London Hospitals NHS Foundation Trust, London, UK

<sup>8</sup>Department of Radiology, Ege University Hospital, Izmir, Turkey

<sup>9</sup>Lungs for Living Research Centre, UCL, London, UK

<sup>10</sup>UCL Respiratory, University College London, London, UK

<sup>11</sup>Respiratory Medicine, Royal Free London NHS Foundation Trust, London, UK

Corresponding author:

Dr Joseph Jacob

UCL Centre for Medical Image Computing

1st Floor, 90 High Holborn, London WC1V6LJ

[j.jacob@ucl.ac.uk](mailto:j.jacob@ucl.ac.uk)

## **Abstract**

The morphology and distribution of airway tree abnormalities enables diagnosis and disease characterisation across a variety of chronic respiratory conditions. In this regard, airway segmentation plays a critical role in the production of the outline of the entire airway tree to enable estimation of disease extent and severity. In this study, we propose a data-centric deep learning technique to segment the airway tree. The proposed technique utilises interpolation and image split to improve data usefulness and quality. Then, an ensemble learning strategy is implemented to aggregate the segmented airway trees at different scales. In terms of segmentation performance (dice similarity coefficient), our method outperforms the baseline model by 2.5% on average when a combined loss is used. Further, our proposed technique has a low GPU usage and high flexibility enabling it to be deployed on any 2D deep learning model.

## Introduction

Abnormal dilatation of the airways is a key feature in the diagnosis of idiopathic pulmonary fibrosis (IPF) patients. Disease extent and severity in IPF can be assessed by visual analysis of high-resolution CT images by radiologists. This approach, however, is subjective and time consuming. Automated airway tree analysis is an alternative method which enables an objective quantitative assessment of airway damage and therefore disease severity in IPF. The key component of airway tree analysis is establishing the 3D geometry of the airway tree and the standard approach to obtain the airway tree is image segmentation.

Airway segmentation is an active research area [1]. The goal is to produce a complete airway tree including the trachea, bronchi, bronchioles and terminal bronchioles. The segmentation task is challenging as the intensity, scale/size and shape of airway segments and their walls change across generations. Classical segmentation methods such as the Frangi filter [2, 3] and region growing method [4] were first used to segment the airway tree. The Frangi enhancement filter constructs a Hessian matrix to extract tubular-like tissues (i.e., airways) and remove non-tubular tissues (i.e. lung). This approach shows promise on airway segmentation. However, the segmented airway tree is limited to the first few branching airway generations (i.e. between 1<sup>st</sup> and 6<sup>th</sup> generations). Furthermore, it requires tuning the parameters ( $\alpha$ ,  $\beta$  and  $\sigma$ ) manually for extracting the optimal airway tree. This process is time-consuming and not user-friendly for clinicians. Employing a region growing algorithm is another approach to segment the airway tree. A seed point is first placed at the trachea, then the region is grown by adding neighbour voxels with a predefined intensity. The algorithm stops when no more voxels can be added. There are several drawbacks to this approach. Intensity thresholding is used to select voxels, but causes leakage (over-segmentation) when an aggressive threshold is used. Conversely, the airway is under segmented when a conservative threshold is used. Therefore, the completeness of the airway tree produced by this approach is limited.

Recent advances in deep learning provides new opportunities for segmentation. It utilises data and GPU technology and offers a fast and fully automatic method to perform segmentation. Deep learning can be divided into two branches – (1) Model-centric and (2) Data-centric. Model-centric deep learning focuses on the model architecture and keep the data unchanged. Popular models have been developed to tackle segmentation challenge. For examples, SegNet [5] and HRNet [6] are proposed for general segmentation. Unet [7] and Vnet [8] are deployed for medical image segmentation. These models produce a good segmentation though they require high GPU memory usage. On the other hand, data-centric deep learning focuses on the data and keeps the model unchanged. Data augmentation [9] is an example of manipulating the source data to produce more varied samples. It uses geometrical transformation (i.e., flip, rotate and crop) to modify the images. The model performance can be improved by training on a dataset with richer features. Active learning [10] is another example of a data-centric technique. It aims to select the most useful data for labelling and permits the user to interact with the deep learning model to complete the data annotation. This technique improves the efficiency of the annotation task. Furthermore, a data-centric deep learning approach is particularly attractive as it requires low GPU memory usage and its approach is straightforward to implement.

The studies related to model-centric deep learning in airway segmentation are summarised below. A convolutional neural network (CNN) based leak detection method to improve airway segmentation was proposed by Charbonnier et al [11]. Yun et al [12] presented a 2.5D CNN for airway segmentation. This approach achieved about 90% DSC accuracy. A 3D Unet to detect topological leak was employed by Nadeem et al. [13]. The intensity threshold was adjusted on the probability map and a freeze-and-growth algorithm was used to correct the leaks. Qin et al. [14] developed a simple-yet-effective deep learning method for this task. It utilised a context-scale fusion strategy to improve the connectivity between airway segments. The DSC of this approach is 93% on a public dataset. A three-dimensional multi-scale feature aggregation network was proposed by Zhou et al. [15] to handle the difference in scale of substructures during airway tree segmentation. This method produced results with 86.18% DSC and 79.31% true positive rate (TPR). Further, a simple and low-memory 3D Unet was developed by Garcia-Uceda et al. [16]. It processed large 3D image patches in a single pass within the network creating a robust and efficient analysis. Zheng et al. [17] proposed WingsNet with group supervision to deal with class imbalance between airway and non-airway regions. The branch detection rate of the proposed method is 80.5%. A coarse-to-fine segmentation framework was deployed by Guo et al. [18]. This utilised a multi-information fusion convolution neural network (Mif-CNN) and a CNN-based region growing for main airway and small branch segmentation. The DSCs of this work were 93.5% and 95.8% for private and public datasets respectively. Wang et al. [19] developed a spatial fully connected tubular network with a novel radial distance loss for 3D tubular-structure segmentation. The method provided a better airway tree segmentation than the baseline Unet model. A joint 3D UNet-Graph Neural Network-based method was presented by Juarez et al. [20]. It used graph convolutions to improve airway connectivity. More recently, Zheng et al. [17] identified the gradient erosion and dilation problem and designed a group supervision to enhance the training of the network. A general union loss was also developed to tackle the intra-class imbalance issue through distance-based weights and element-wise focus on the hard-to-segment regions. Wu et al. [21] proposed a long-term slice propagation method for airway segmentation. The method achieved 92.95% DSC. A novel label refinement method was developed by Chen et al. [22] to correct the structural errors in airway segmentation. It produced an airway segmentation with DSC between 79% and 81%. Zhao et al. [23] developed Group Deep Dense Supervision for small bronchiole segmentation. This method has a high sensitivity in detecting fine-scale branches and outperforms state-of-the-art methods by a large margin (+12.8% in Branch Detection and +8.8% in Tree Detection).

Currently, no study focuses on a purely data-centric approach for airway segmentation. Therefore, in this study, we propose a 2D data-centric deep learning method for the automated segmentation of airway trees on HRCT images. The proposed technique is evaluated by comparing the segmentation performance with a baseline model (2D Dilated Unet).

The main contributions of this study are:

- The first study to propose a 2D data-centric deep learning method with interpolation that segments the airways on HRCT images.

- The proposed technique utilises interpolation and image split to improve data usefulness and quality.
- An ensemble learning strategy is implemented to aggregate the segmented airway trees at different scales.
- The proposed technique has a low GPU usage and high flexibility to be deployed in any 2D deep learning model.

## **Methods**

### *Data pre-processing*

The data were pre-processed in three steps: (1) ImageJ was used to convert the source images from DICOM format to TIFF format. (2) The images were subsequently normalised by using the following settings to emphasize lung tissue visualisation:  $W = 1500$  HU,  $L = -500$  HU. (3) The intensity of the normalised images were rescaled in the range 0 to 255HU. The annotation of the ground-truth mask was performed on 3D Slicer.

### *Model development*

The airway was segmented by using a modified dilated Unet. A dilated Unet is an extended model of the original Unet [7] and adopts an encoder-decoder architecture. The encoding path captures features from images and the decoding path localises these features. A sequential dilation module [24] is employed in the bottleneck layer and this improves global context capturing and maintains the resolution of the feature map. Furthermore, the dilated Unet was modified by introducing batch normalisation and dropout. These modifications improve model stability and segmentation performance. The schematic diagram of the dilated Unet and the sequential dilation module are shown in Figures 1 and 2.

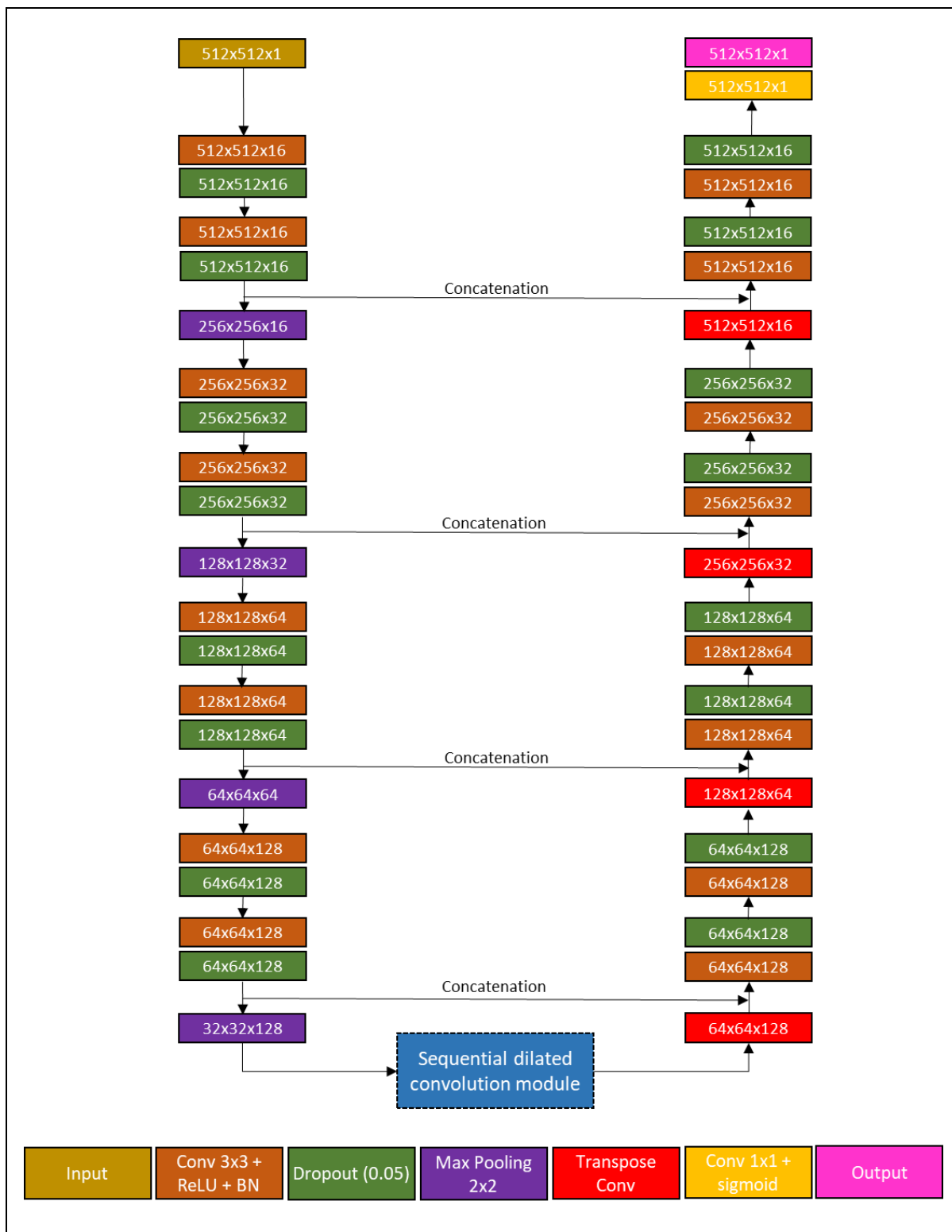


Figure 1: The network architecture of the proposed method.

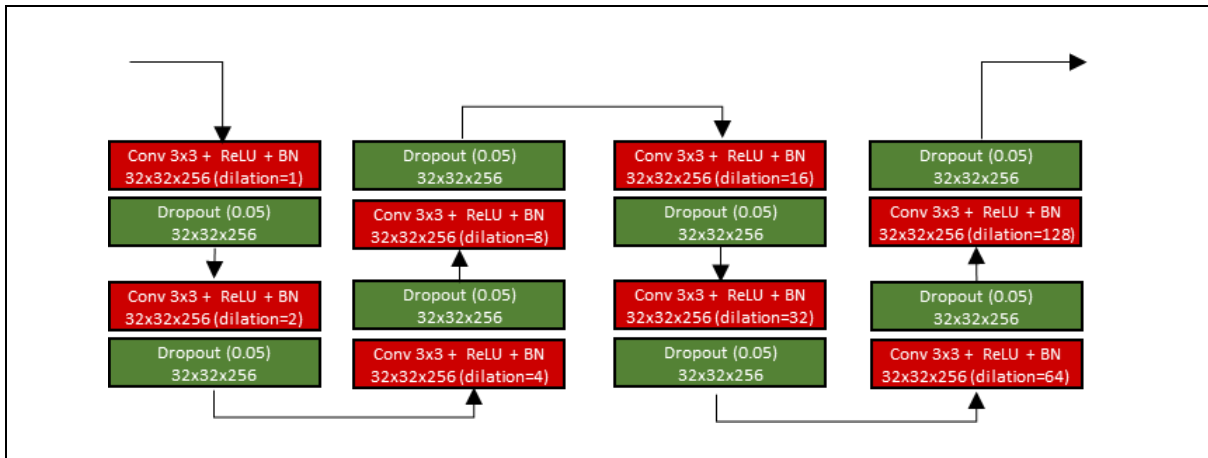


Figure 2: The sequential dilated convolution module.

### Interpolation and split

A new data-centric technique is introduced in this study. The CT image and its mask are zoomed in at various scales. The zoomed-in CT images and masks are produced by interpolation and split. The original CT images are up-sampled by bi-linear interpolation, while the original masks are up-sampled by nearest neighbour interpolation. Then, the interpolated image is split into sub-images with fixed dimensions (512x512). Here, an interpolation ratio ( $ir$ ) is defined to control the zoom-in scale. For example, the dimension of the interpolated image (1024x1024) is doubled from the original image (512x512) when  $ir$  is set to 2. Then, the interpolated image is split into four sub-images (512x512). The interpolation and split mechanism (i.e.,  $ir2$ ) is demonstrated in Figure 3. Further, the effect of the interpolated ratio ( $ir = 2, 4$  and  $8$ ) is investigated. It should be noted that no interpolation and split is performed for  $ir = 1$ .

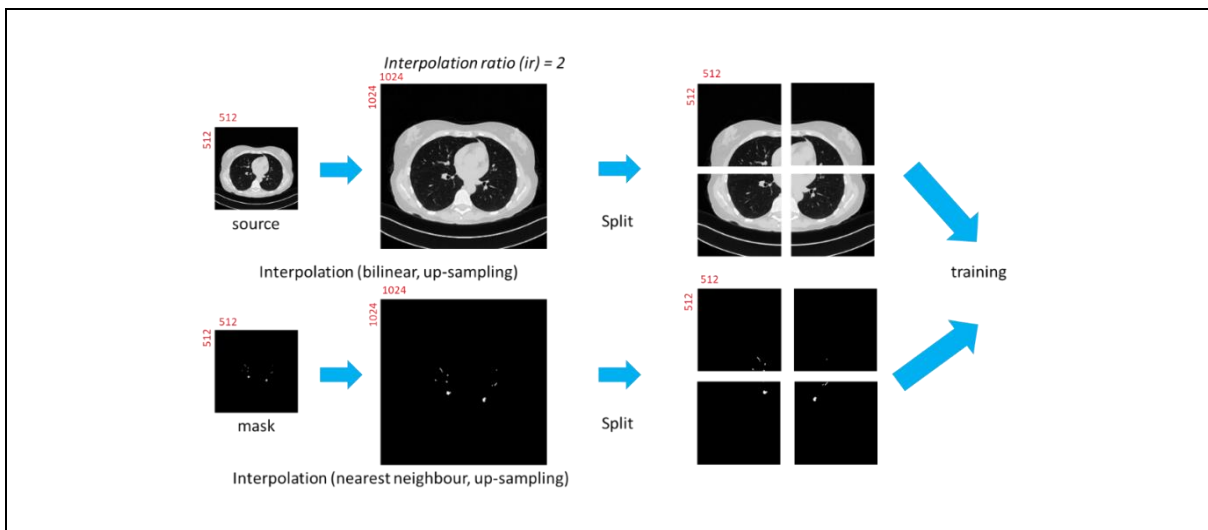


Figure 3: The interpolation and split mechanism.



### Implementation and training strategy

The clinical data ( $n = 25$ ) contained healthy subjects, patients with heart disease and patients with IPF. It included 2 patients with heart disease from the EXACT09 dataset [25], 6 healthy never-smoker subjects and 17 IPF patients from University College London Hospital. The study was carried out in accordance with the recommendations of University College London Research Ethics Committee, with written informed consent from all subjects. The data including source images and their ground-truth masks were further divided into training (80%) and validation (20%) sets. Table 1 shows the subject/patient information in the validation set. The number of samples (source images) for training and validation is shown in Table 2.

Table 1: The subject/patient information in the validation set.

<b>Subject/Patient</b>	<b>Status</b>
Subject 1	Healthy
Subject 2	Healthy
Patient 1	Patient with IPF
Patient 2	Patient with heart disease
Patient 3	Patient with IPF

Table 2: The number of samples (source images) for training and validation.

<b>Interpolation ratio (<math>ir</math>)</b>	<b>Training set</b>	<b>Validation set</b>
<b>1</b> <b>(original dataset)</b>	7552	1995
<b>2</b>	30208	7980
<b>4</b>	120832	31920
<b>8</b>	483328	127680

The proposed models (per  $ir$ ) were trained and implemented on a high performance cluster with deep learning frameworks installed. Specifically, Tensorflow (v1.1.4) and Keras (v2.2.4) were executed on Linux (Rocks 7). Furthermore, various computing machines with Intel/AMD multi-core CPU chipset and Nvidia GPU cards were used to complete the training.

The final trained models were produced by employing the Adam optimiser, ReduceLROnPlateau and Early stopping. The setting of parameters is shown in Table 3.

Table 3: The setting of parameters for models training.

<b>Adam optimiser</b>	
Learning rate (initial)	$10^{-3}$
Epochs	200
<b>ReduceLROnPlateau</b>	
Factor	$10^{-1}$
Patience	3
Min_lr	$10^{-5}$
<b>Early stopping</b>	
Patience	10

Two loss functions, combined loss and focal loss, were used to train the baseline model. The combined loss function includes binary cross entropy (BCE) and dice similarity coefficient (DSC). The BCE is used to calculate the difference between the two probability distributions (foreground vs background). DSC is used to measure the similarity between predicted segmentation and the ground-truth segmentation.

Focal loss is commonly used to deal with the class imbalance. It generalizes the BCE and a focusing parameter, gamma, is introduced to penalize more heavily on hard-to-classify samples relative to easy-to-classify samples. The settings are alpha = 0.25 and gamma = 2.

The prediction (per *ir*) was done using the trained models above. The unseen source images were interpolated and split to form the inputs for model prediction. When the prediction was complete, the initial predicted masks were merged and down-sampled (nearest neighbour) to the final mask with size 512x512. The workflow of the prediction mechanism (i.e., ir1 + ir2) is shown in Figure 4.

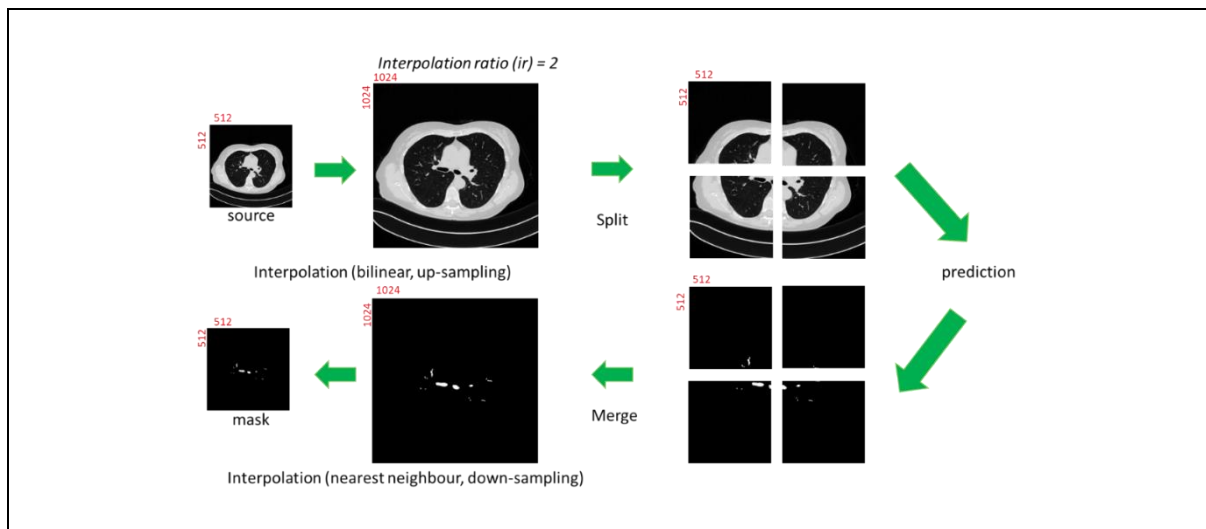


Figure 4: The workflow of prediction mechanism.

### *Ensemble learning strategy*

An ensemble learning strategy is employed to improve the airway segmentation performance. The segmented masks from  $ir = 1, 2, 4$  and  $8$  are aggregated to form a combined mask. This is done by applying a union operation on all mask sets. Finally, the largest connected component of an airway in the combined mask is extracted and hence the final segmented mask is produced. The workflow of this ensemble learning strategy (i.e.,  $ir1 + ir2 + ir4 + ir8$ ) is shown in Figure 5.

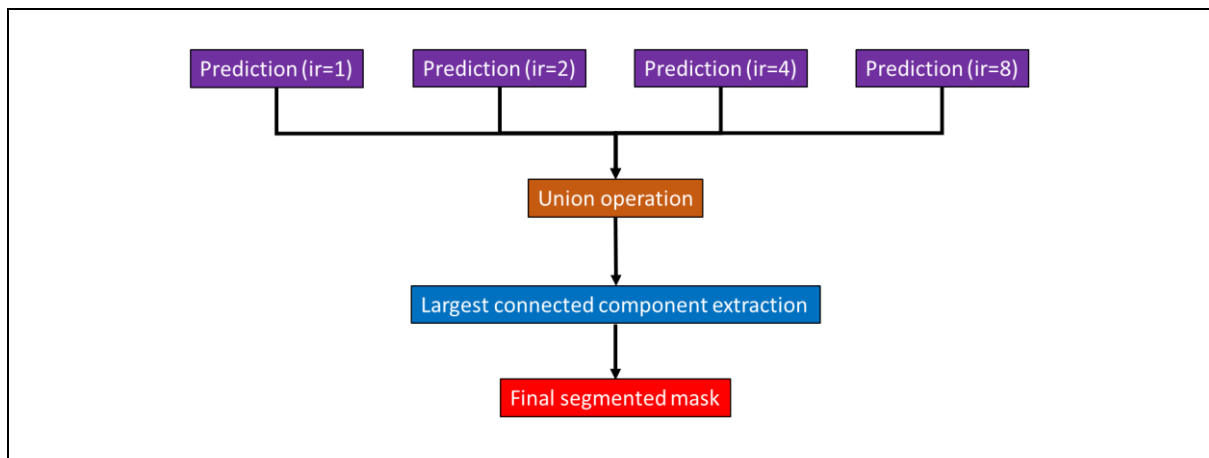


Figure 5: The workflow of ensemble learning strategy.

## Results

### *Learning and validation performance*

The learning and validation performance are showed in Table 4. In the training set, both losses are low and the losses tend to reduce when the interpolation ratio increases. In contrast, these losses are slightly higher in the validation set and no overfitting is observed.

Table 4: Learning and validation performance for combined loss and focal loss.

	Training set		Validation set	
	Combined loss	Focal loss	Combined loss	Focal loss
<b>ir1</b>	0.07	$1.58 \times 10^{-4}$	0.13	$2.28 \times 10^{-4}$
<b>ir2</b>	0.08	$2.23 \times 10^{-4}$	0.16	$3.73 \times 10^{-4}$
<b>ir4</b>	0.03	$2.03 \times 10^{-4}$	0.07	$3.82 \times 10^{-4}$
<b>ir8</b>	0.07	$2.88 \times 10^{-4}$	0.04	$4.94 \times 10^{-4}$

### *Airway segmentation performance*

Tables 5 and 6 show the airway segmentation performance by using combined loss and focal loss respectively. Our proposed data-centric method provides a better airway segmentation compared to a baseline model (ir1) for both losses. On average, our method (ir1 + ir2 + ir4 + ir8) with combined loss has the highest DSC (84.26%). Furthermore, our method with focal loss has the highest DSC (81.17%). In particular, our method with combined loss performs better than the one with focal loss in airway segmentation.

Table 5: Airway segmentation performance in percentage (Combined loss).

DSC	Subject 1	Subject 2	Patient 1	Patient 2	Patient 3	Average $\pm$ SD
<b>ir1</b>	85.27	81.56	78.99	83.20	79.71	$81.74 \pm 2.57$
<b>ir1 + ir2</b>	85.93	82.12	80.34	85.51	83.38	$83.45 \pm 2.34$
<b>ir1 + ir2 + ir4</b>	86.06	82.27	80.80	86.75	84.67	$84.11 \pm 2.52$
<b>ir1 + ir2 + ir4 + ir8</b>	86.10	81.81	81.40	86.75	85.21	$84.26 \pm 2.49$

Table 6: Airway segmentation performance in percentage (Focal loss).

DSC	Subject 1	Subject 2	Patient 1	Patient 2	Patient 3	Average $\pm$ SD
<b>ir1</b>	82.02	77.67	77.51	81.51	77.55	$79.25 \pm 2.30$
<b>ir1 + ir2</b>	82.71	78.08	78.07	82.73	78.24	$79.97 \pm 2.51$
<b>ir1 + ir2 + ir4</b>	82.88	78.28	78.27	83.75	82.02	$81.04 \pm 2.60$
<b>ir1 + ir2 + ir4 + ir8</b>	82.93	78.29	78.49	84.13	82.03	$81.17 \pm 2.65$

The airway segmentation results of subject 1, patient 2 and patient 3 are shown in Figures 6, 7 and 8. Our method with combined loss achieves 86.10%, 86.75% and 85.21% DSC respectively, while the method with focal loss achieves 82.93%, 84.13% and 82.03% DSC respectively. Visually, the trachea and bronchi are well segmented for both losses. The majority of bronchioles are better segmented by our method with combined loss.

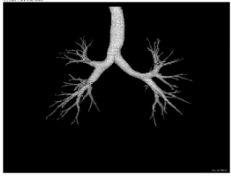
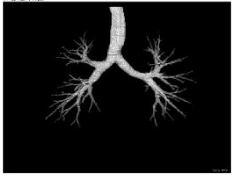
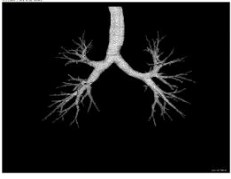
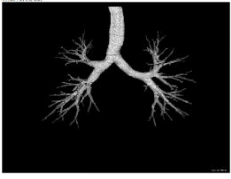
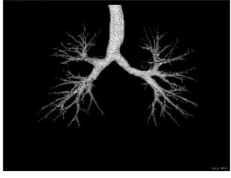
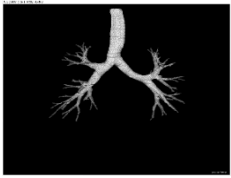
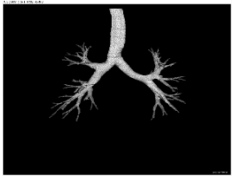
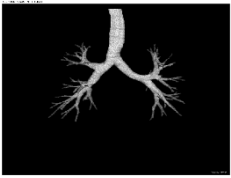
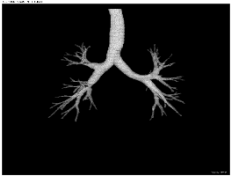
Loss function	ir1	ir1 + ir2	ir1 + ir2 + ir4	ir1 + ir2 + ir4 + ir8	Ground-truth
Combined loss					
Focal loss					

Figure 6: Airway segmentation (3D display, combined loss) of subject 1.

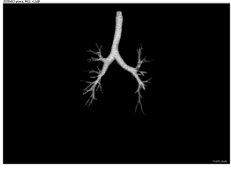
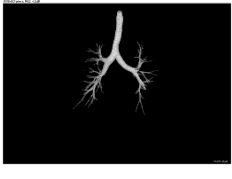
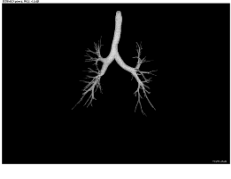
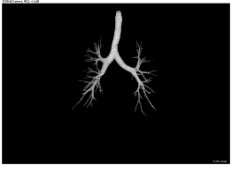
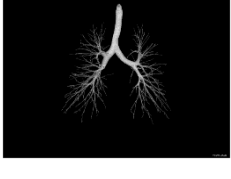
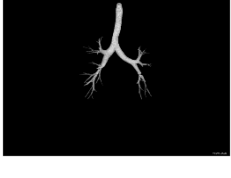
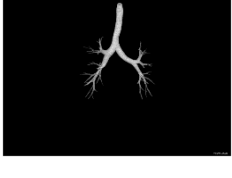


Loss function	ir1	ir1 + ir2	ir1 + ir2 + ir4	ir1 + ir2 + ir4 + ir8	Ground-truth
Combined loss					
Focal loss					

Figure 7: Airway segmentation (3D display, combined loss) of patient 2.

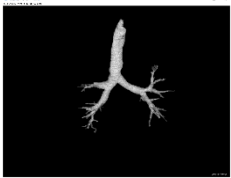
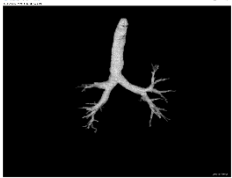
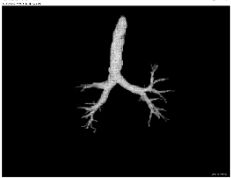
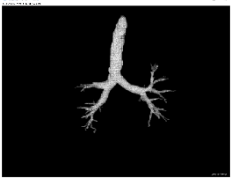
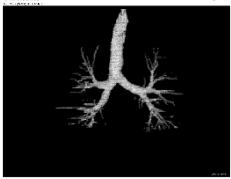
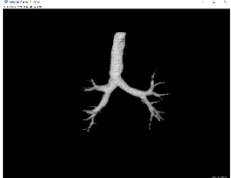
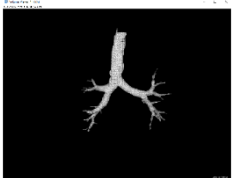
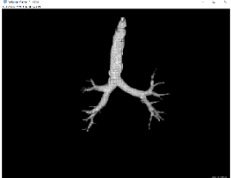
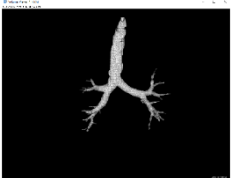
Loss function	ir1	ir1 + ir2	ir1 + ir2 + ir4	ir1 + ir2 + ir4 + ir8	Ground-truth
Combined loss					
Focal loss					

Figure 8: Airway segmentation (3D display, combined loss) of patient 3.

### *Airway segmentation performance gain*

The airway segmentation performance gain (expressed as a percentage) by using our method with combined loss and focal loss are reported in Tables 7 and 8. Our method (ir1 + ir2 + ir4 + ir8) with combined loss has the highest average percentage gain (2.51%). Notably, patients 2 and 3 have relatively high performance gain and their percentage gains are 3.56% and 5.50%. The segmentation performance gain is further improved when segmentation with a higher interpolation ratio is aggregated. Furthermore, the airway segmentation performance gain in percentage by using our method with focal loss shows a similar trend but has a lower gain than the method with combined loss.

Table 7: Airway segmentation performance gain in percentage (Combined loss).

<b>DSC</b>	<b>Subject 1</b>	<b>Subject 2</b>	<b>Patient 1</b>	<b>Patient 2</b>	<b>Patient 3</b>	<b>Average <math>\pm</math> SD</b>
<b>ir1 + ir2</b>	0.66	0.56	1.35	2.31	3.67	1.71 $\pm$ 1.30
<b>ir1 + ir2 + ir4</b>	0.79	0.72	1.81	3.55	4.96	2.37 $\pm$ 1.85
<b>ir1 + ir2 + ir4 + ir8</b>	0.84	0.26	2.41	3.56	5.50	2.51 $\pm$ 2.12

Table 8: Airway segmentation performance gain in percentage (Focal loss).

<b>DSC</b>	<b>Subject 1</b>	<b>Subject 2</b>	<b>Patient 1</b>	<b>Patient 2</b>	<b>Patient 3</b>	<b>Average <math>\pm</math> SD</b>
<b>ir1 + ir2</b>	0.68	0.41	0.55	1.22	0.69	0.71 $\pm$ 0.31
<b>ir1 + ir2 + ir4</b>	0.85	0.61	0.75	2.24	4.47	1.79 $\pm$ 1.64
<b>ir1 + ir2 + ir4 + ir8</b>	0.90	0.62	0.97	2.62	4.47	1.92 $\pm$ 1.63

Figure 9 shows the comparison of airway segmentation between our method (ir1 + ir2 + ir4 + ir8) and the baseline model (ir1) for subject 1, patient 2 and patient 3. It is clear that our method segments more bronchioles than the baseline model. Furthermore, our method improves the airway wall segmentation for patient 3.

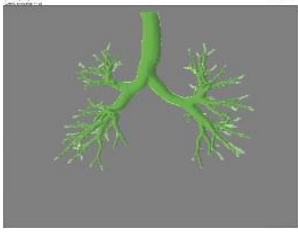
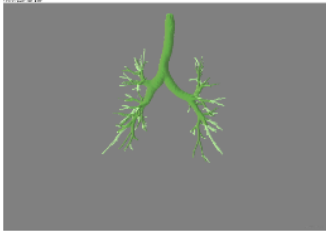
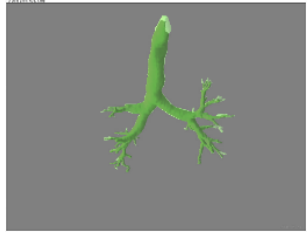

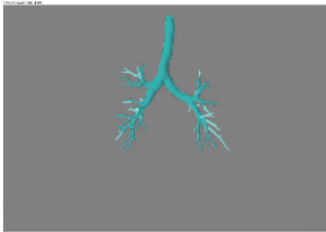
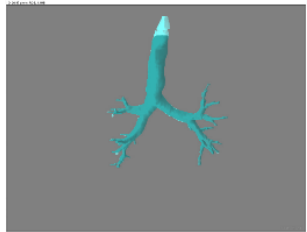
Loss function	Subject 1	Patient 2	Patient 3
Combined loss			
Focal loss			

Figure 9: The comparison of airway segmentation between our method (ir1 + ir2 + ir4 + ir8 - light green / light blue) and the baseline model (ir1 - green / blue) for subject 1, patient 2 and patient 3.

### *Effect of interpolation ratio (ir)*

The effect of interpolation ratio for subject 1, patient 2 and patient 3 is illustrated in Figure 10. By observing the segmented airways from ir1 to ir8, more bronchioles are segmented. Furthermore, when the highest interpolation ratio ( $ir = 8$ ) is used, the segmentation of the trachea is the worst. In general, more artefacts are observed when a higher interpolation ratio is used.

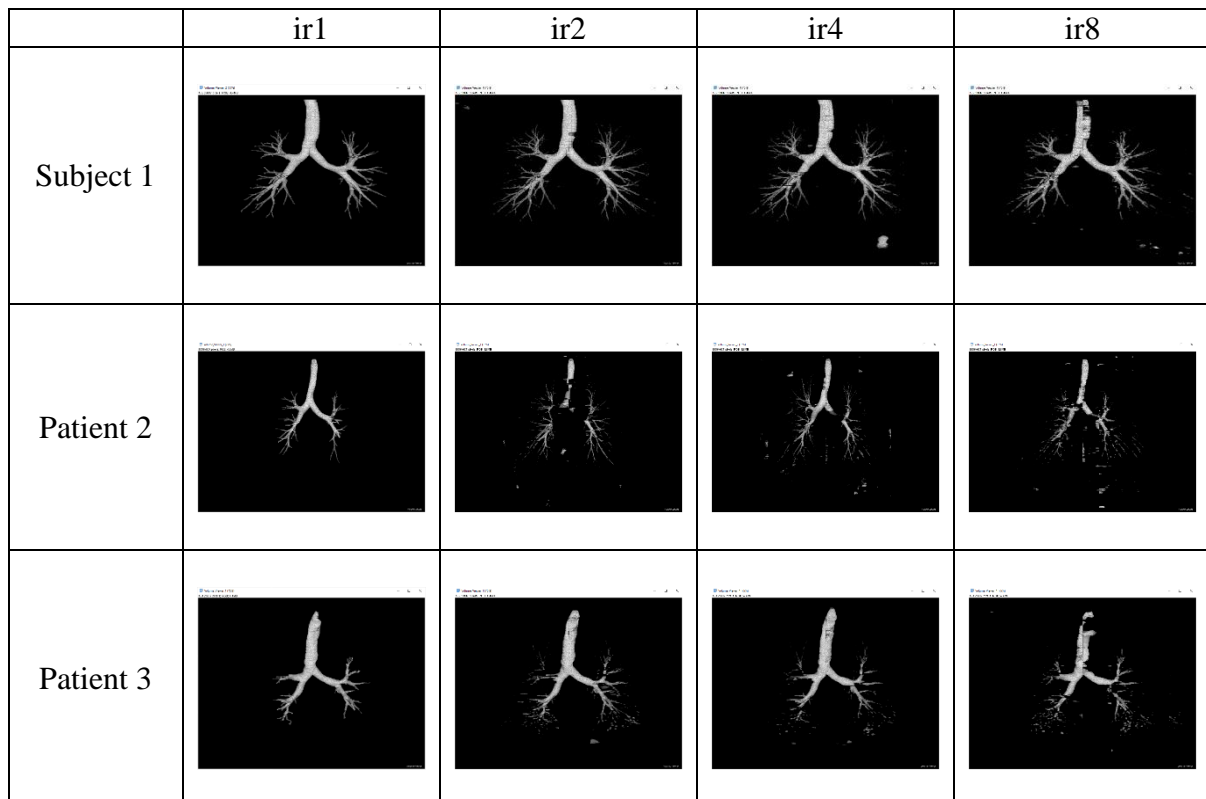


Figure 10: Effect of interpolation ratio for subject 1, patient 2 and patient 3 (combined loss).

### *Blur effect*

The blur effect of our method is illustrated in Figure 11. The blur level is increased with increasing interpolation ratio. It is visually evident when the interpolation ratio is set at 4 and 8. Though the size of the bronchiole is increased after interpolation, the sharpness of the bronchiole wall is reduced. Furthermore, the blur effect is not visually evident when the interpolation ratio is set at 2.



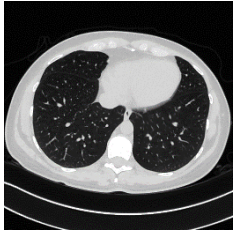
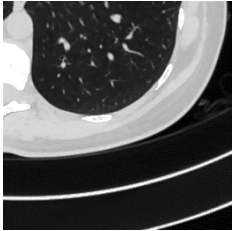
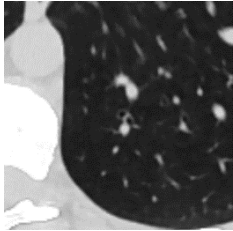
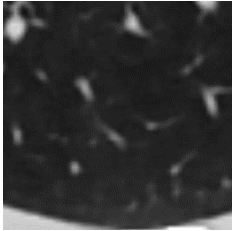
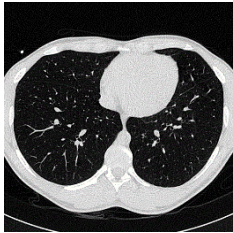
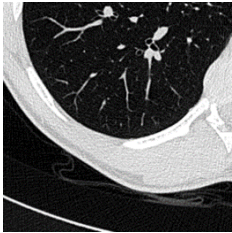
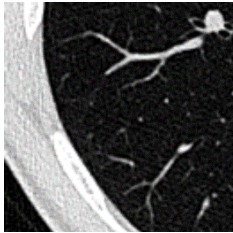
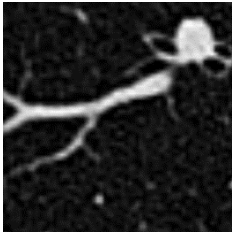
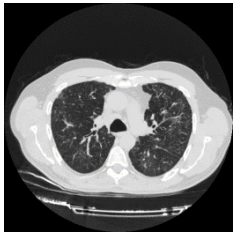
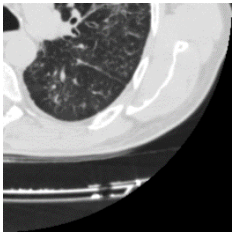
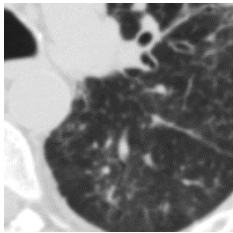
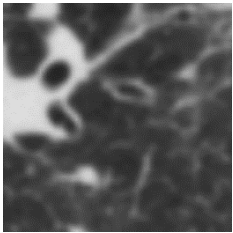
	ir1	ir2	ir4	ir8
Subject 1				
Patient 2				
Patient 3				

Figure 11: The blur effect of our method for subject 1, patient 2 and patient 3.

Regarding the blur effect of our method, a sharpening filter (Figure 12) can be used to reduce this effect and further improve the segmentation accuracy by about 1%.

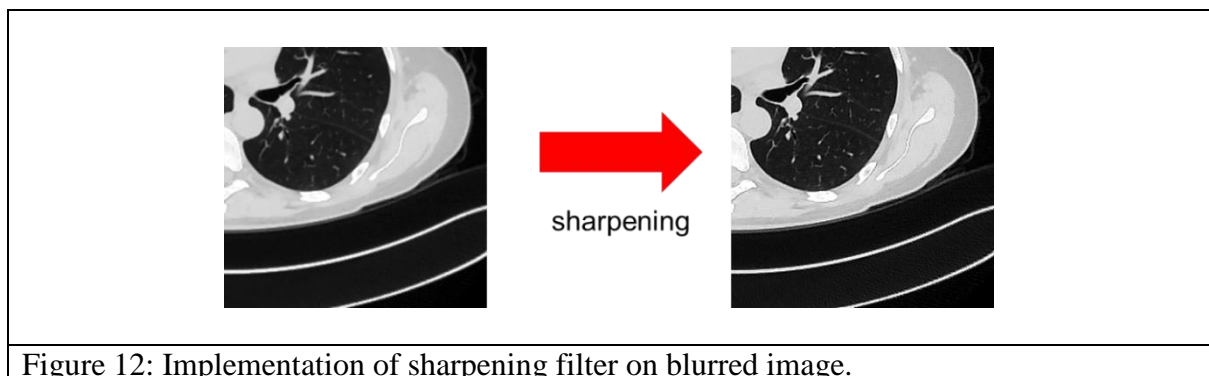


Figure 12: Implementation of sharpening filter on blurred image.

### Effect of ensemble learning strategy

The effect of the ensemble learning strategy can be visualised by investigating 2D segmented airway masks. Figures 13, 14 and 15 show the selected 2D masks of airway segmentation (combined loss) for subject 1, patient 2 and patient 3 respectively. For subject 1, the segmentation of bronchi is gradually improved from ir1 to ir1 + ir2 + ir4 + ir8. The connection between bronchi is also improved. Further, higher generation bronchioles are able to be segmented. In the case of patient 2, the segmentation improvement can be observed from subsegmental bronchi to bronchioles. For patient 3, the segmentation of primary bronchi is improved. Additionally, some subsegmental bronchi are better segmented.

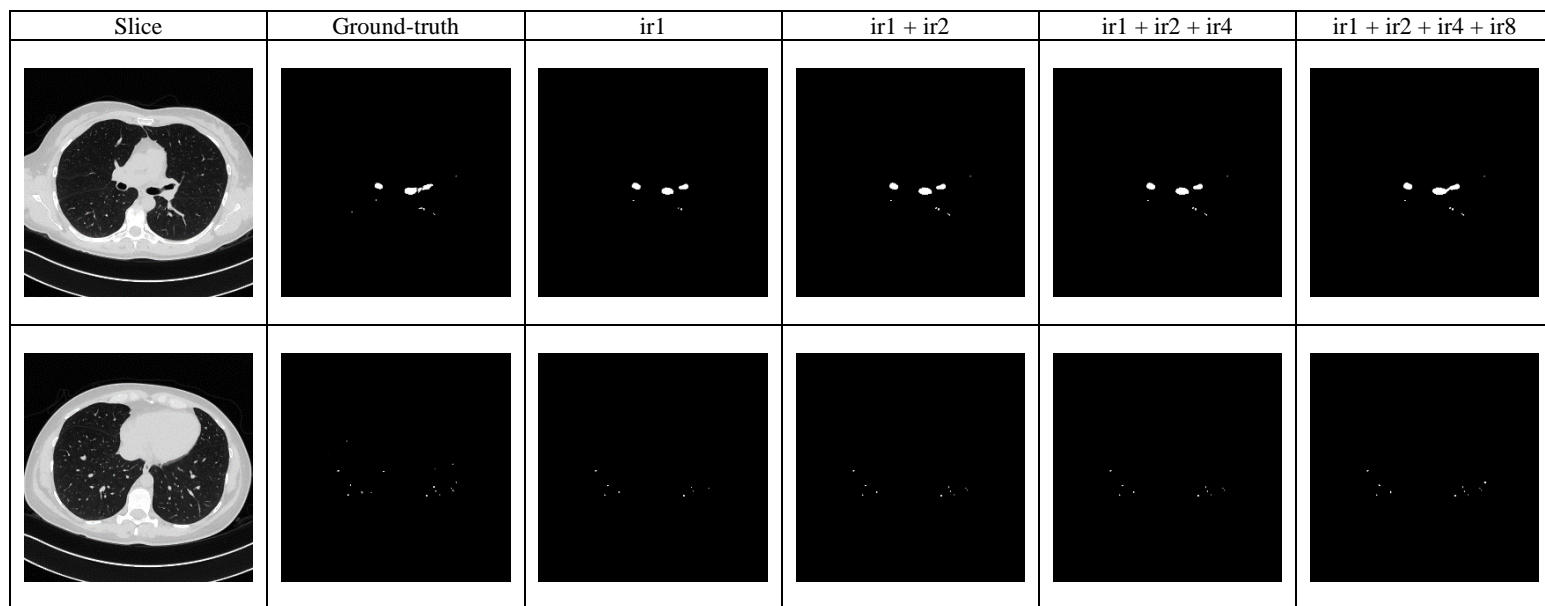


Figure 13: Selected 2D masks of airway segmentation (combined loss) for subject 1.

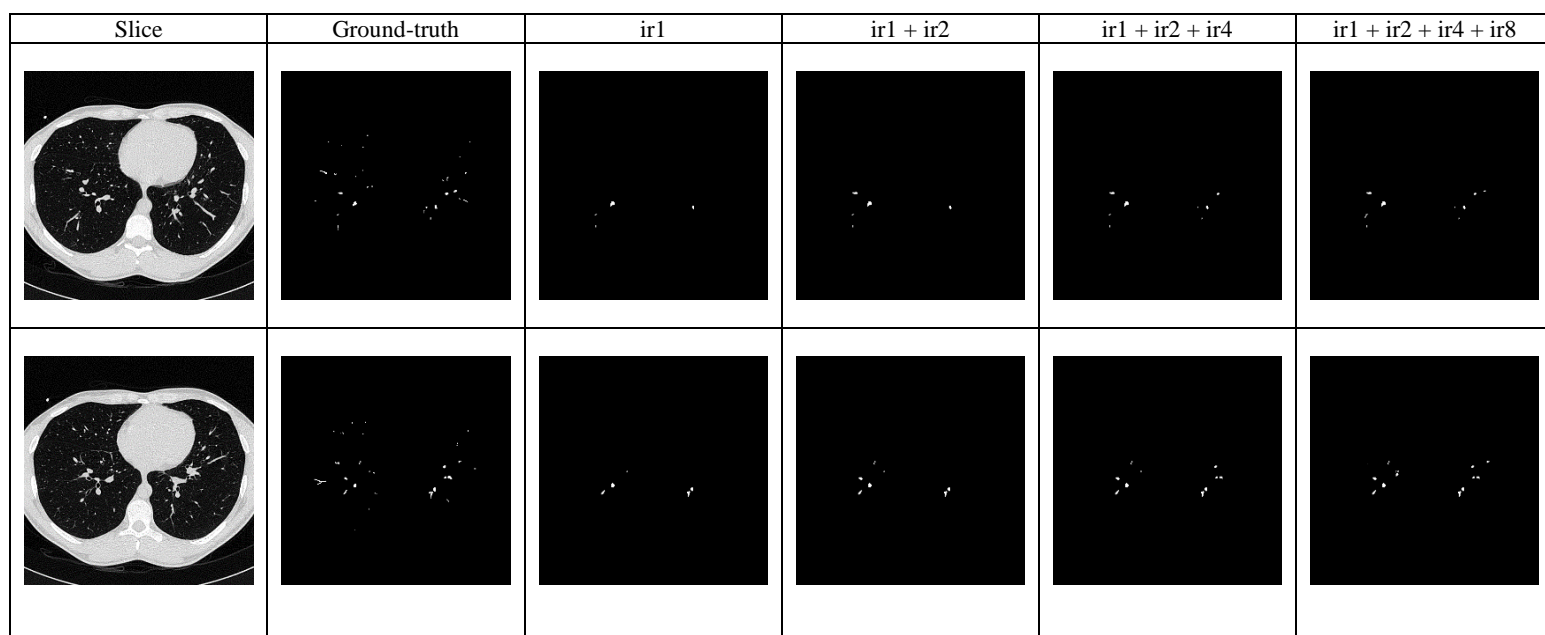


Figure 14: Selected 2D masks of airway segmentation (combined loss) for patient 2.

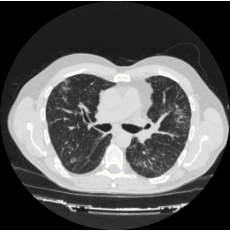





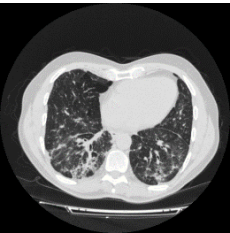
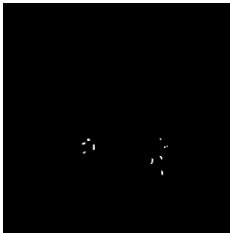
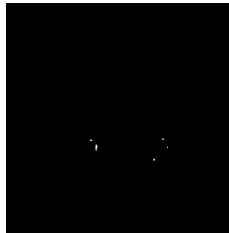
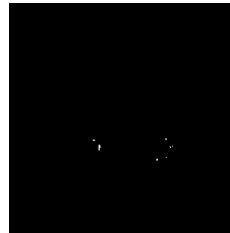
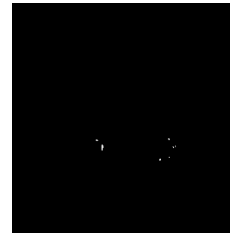

Slice	Ground-truth	ir1	ir1 + ir2	ir1 + ir2 + ir4	ir1 + ir2 + ir4 + ir8
					
					

Figure 15: Selected 2D masks of airway segmentation (combined loss) for patient 3.

## Discussion

A data-centric deep learning method has been developed to improve airway segmentation on high resolution CT images. The proposed method can be applied to any 2D deep learning model including standard models, such as the U-net and Res-net. Our study shows that the airway segmentation performance gain is between 0.26% and 5.50%.

The proposed method is good at improving (1) the connectivity between airway segments (2) airway wall segmentation (3) bronchi and bronchioles segmentation. It utilises zoom-in images and aggregates the segmented airways at different scales. The zoom-in images are useful for the model to capture the features of the walls of large airways and segment more small airways which are shape and scale/size dependent [26]. Further, the ensemble learning strategy combines the airway segmentation at various interpolation ratios and hence improves the connectivity between airway segments.

In this study, we observe that the interpolation ratio affects the airway segmentation. Although more small airways are detected and segmented, the large airways such as the trachea and primary bronchi are not segmented well at higher interpolation ratios. This implies that an optimal scale/size range of airways exists for a given interpolation ratio. The higher interpolation ratio shifts the optimal scale/size range towards smaller airways.

It should be noted that the current study uses the threshold (0.5) for binarization. We also observe that changing the interpolation ratio affects the threshold. A further study is required to investigate the relationship between optimal threshold and interpolation ratio. We also noted

that the sample size increases significantly with higher interpolation ratios and hence the training time increases accordingly. Data parallelism can be deployed to speed up the training and maintain the computational efficiency.

Two loss functions have been studied in this work. In terms of segmentation accuracy and gain, the combined loss performs better than the focal loss. However, it should be noted that the false positive rate of focal loss is lower than the combined loss. This suggests that focal loss can be used as a more conservative way to obtain the airway tree. Also, it may be possible to produce an airway segmentation with high accuracy and low false positive rate when the combination of these two losses is used.

A human tracheobronchial tree has 23 airway generations on average [27, 28]. High-resolution CT has the ability to image a smaller component of the airway tree as bronchioles with a diameter less than 2mm are not visible on HRCT. In health up to 8 airway generations may be visible on HRCT [29], and the number of visible airway generations increases in disease states. The segmentation performance of normal subjects was compared with IPF patients. Notably, our proposed method shows better performance gain on IPF patients. This might be explained by the observation that more abnormal small airways (between the 9th and 13th airway generations) [30] are found in IPF patients. This also reveals that our method improves the segmentation of small airways.

In this study, a dilated U-net is chosen to be the baseline model as its segmentation performance is better than a U-net. The segmentation performance of U-net is about 75% [31], while the dilated U-net achieves about 80% segmentation accuracy. This also demonstrates the benefits and usefulness of the proposed technique applied to a more complex model.

Our study has several limitations. First, the subjects and patients were selected retrospectively. This might introduce the bias on data selection. Second, manual annotation was performed to produce ground-truth labels for airway tree segmentation. The annotators might bias the accuracy of the ground-truth labels. Third, the segmentation performance metric, DSC, might provide a biased measurement as the large and small airways were examined together. Larger airways segmented well might have resulted in a good DSC even if small airways were segmented poorly.

## **Conclusion**

Our study is the first to demonstrate the feasibility of using a data-centric deep learning method to segment the airway tree resulting in a good segmentation performance gain. Our method maintains GPU memory efficiency and has the flexibility to be deployed in any 2D deep learning model. Future work should investigate 3D data-centric approaches for their segmentation performance gain.

## Acknowledgement

JJ was supported by Wellcome Trust Clinical Research Career Development Fellowship 209553/Z/17/Z and the NIHR Biomedical Research Centre at University College London. This research was funded in whole or in part by the Wellcome Trust [209553/Z/17/Z]. For the purpose of open access, the author has applied a CC-BY public copyright licence to any author accepted manuscript version arising from this submission.

## Declaration of Interest

JJ declares fees from Boehringer Ingelheim, F. Hoffmann-La Roche, GlaxoSmithKline, NHSX, Takeda, Wellcome Trust, Microsoft Research unrelated to the submitted work and UK patent application numbers 2113765.8 and GB2211487.0.

## References

- [1] M. Zhang *et al.*, "Multi-site, Multi-domain Airway Tree Modeling (ATM'22): A Public Benchmark for Pulmonary Airway Segmentation," *arXiv preprint arXiv:2303.05745*, 2023.
- [2] A. F. Frangi, W. J. Niessen, K. L. Vincken, and M. A. Viergever, "Multiscale vessel enhancement filtering," (in English), *Medical Image Computing and Computer-Assisted Intervention - Miccai'98*, vol. 1496, pp. 130-137, 1998, doi: DOI 10.1007/bfb0056195.
- [3] S. You, E. Bas, and D. Erdogmus, "Extraction of samples from airway and vessel trees in 3D lung CT based on a multi-scale principal curve tracing algorithm," *Annu Int Conf IEEE Eng Med Biol Soc*, vol. 2011, pp. 5157-60, 2011, doi: 10.1109/IEMBS.2011.6091277.
- [4] H. H. Duan, J. Gong, X. W. Sun, and S. D. Nie, "Region growing algorithm combined with morphology and skeleton analysis for segmenting airway tree in CT images," *J Xray Sci Technol*, vol. 28, no. 2, pp. 311-331, 2020, doi: 10.3233/XST-190627.
- [5] V. Badrinarayanan, A. Kendall, and R. Cipolla, "SegNet: A Deep Convolutional Encoder-Decoder Architecture for Image Segmentation," (in English), *Ieee T Pattern Anal*, vol. 39, no. 12, pp. 2481-2495, Dec 2017, doi: 10.1109/Tpami.2016.2644615.
- [6] K. Sun *et al.*, "High-resolution representations for labeling pixels and regions," *arXiv preprint arXiv:1904.04514*, 2019.
- [7] O. Ronneberger, P. Fischer, and T. Brox, "U-Net: Convolutional Networks for Biomedical Image Segmentation," (in English), *Medical Image Computing and Computer-Assisted Intervention, Pt Iii*, vol. 9351, pp. 234-241, 2015, doi: 10.1007/978-3-319-24574-4\_28.
- [8] F. Milletari, N. Navab, and S. A. Ahmadi, "V-Net: Fully Convolutional Neural Networks for Volumetric Medical Image Segmentation," (in English), *Int Conf 3d Vision*, pp. 565-571, 2016, doi: 10.1109/3dv.2016.79.
- [9] C. Shorten and T. M. Khoshgoftaar, "A survey on Image Data Augmentation for Deep Learning," (in English), *J Big Data-Ger*, vol. 6, no. 1, Jul 6 2019, doi: 10.1186/s40537-019-0197-0.

- [10] S. Budd, E. C. Robinson, and B. Kainz, "A survey on active learning and human-in-the-loop deep learning for medical image analysis," *Med Image Anal*, vol. 71, p. 102062, Jul 2021, doi: 10.1016/j.media.2021.102062.
- [11] J. P. Charbonnier, E. M. van Rikxoort, A. A. A. Setio, C. M. Schaefer-Prokop, B. van Ginneken, and F. Ciompi, "Improving airway segmentation in computed tomography using leak detection with convolutional networks," (in English), *Med Image Anal*, vol. 36, pp. 52-60, Feb 2017, doi: 10.1016/j.media.2016.11.001.
- [12] J. Yun *et al.*, "Improvement of fully automated airway segmentation on volumetric computed tomographic images using a 2.5 dimensional convolutional neural net," (in English), *Med Image Anal*, vol. 51, pp. 13-20, Jan 2019, doi: 10.1016/j.media.2018.10.006.
- [13] S. A. Nadeem, E. A. Hoffman, and P. K. Saha, "A Fully Automated CT-Based Airway Segmentation Algorithm using Deep Learning and Topological Leakage Detection and Branch Augmentation Approaches," (in English), *Proc Spie*, vol. 10949, 2019, doi: 10.1117/12.2512286.
- [14] Y. L. Qin, Y. Gu, H. Zheng, M. J. Chen, J. Yang, and Y. M. Zhu, "Airwaynet-Se: A Simple-yet-Effective Approach to Improve Airway Segmentation Using Context Scale Fusion," (in English), *IS Biomed Imaging*, pp. 809-813, 2020. [Online]. Available: <Go to ISI>://WOS:000578080300161.
- [15] K. Zhou *et al.*, "Automatic airway tree segmentation based on multi-scale context information," (in English), *Int J Comput Ass Rad*, vol. 16, no. 2, pp. 219-230, Feb 2021, doi: 10.1007/s11548-020-02293-x.
- [16] A. Garcia-Uceda, R. Selvan, Z. Saghir, H. A. W. M. Tiddens, and M. de Bruijne, "Automatic airway segmentation from computed tomography using robust and efficient 3-D convolutional neural networks," (in English), *Sci Rep-Uk*, vol. 11, no. 1, Aug 6 2021, doi: 10.1038/s41598-021-95364-1.
- [17] H. Zheng *et al.*, "Alleviating Class-Wise Gradient Imbalance for Pulmonary Airway Segmentation," (in English), *Ieee T Med Imaging*, vol. 40, no. 9, pp. 2452-2462, Sep 2021, doi: 10.1109/Tmi.2021.3078828.
- [18] J. Q. Guo *et al.*, "Coarse-to-fine airway segmentation using multi information fusion network and CNN-based region growing," (in English), *Comput Meth Prog Bio*, vol. 215, Mar 2022, doi: 10.1016/j.cmpb.2021.106610.
- [19] C. L. Wang *et al.*, "Tubular Structure Segmentation Using Spatial Fully Connected Network with Radial Distance Loss for 3D Medical Images," (in English), *Medical Image Computing and Computer Assisted Intervention - Miccai 2019, Pt Vi*, vol. 11769, pp. 348-356, 2019, doi: 10.1007/978-3-030-32226-7\_39.
- [20] A. G. U. Juarez, R. Selvan, Z. Saghir, and M. de Bruijne, "A Joint 3D UNet-Graph Neural Network-Based Method for Airway Segmentation from Chest CTs," (in English), *Machine Learning in Medical Imaging (Mlmi 2019)*, vol. 11861, pp. 583-591, 2019, doi: 10.1007/978-3-030-32692-0\_67.
- [21] Y. Q. Wu, M. H. Zhang, W. H. Yu, H. Zheng, J. S. Xu, and Y. Gu, "LTSP: long-term slice propagation for accurate airway segmentation," (in English), *Int J Comput Ass Rad*, vol. 17, no. 5, pp. 857-865, May 2022, doi: 10.1007/s11548-022-02582-7.
- [22] S. Chen *et al.*, "Label Refinement Network from Synthetic Error Augmentation for Medical Image Segmentation," *arXiv preprint arXiv:2209.06353*, 2022.
- [23] M. Zhao *et al.*, "GDDS: Pulmonary Bronchioles Segmentation with Group Deep Dense Supervision," *arXiv preprint arXiv:2303.09212*, 2023.
- [24] F. Yu and V. Koltun, "Multi-Scale Context Aggregation by Dilated Convolutions," *CoRR*, vol. abs/1511.07122, 2016.

- [25] P. Lo *et al.*, "Extraction of airways from CT (EXACT'09)," *IEEE Trans Med Imaging*, vol. 31, no. 11, pp. 2093-107, Nov 2012, doi: 10.1109/TMI.2012.2209674.
- [26] W. K. Cheung, "State-of-the-art deep learning method and its explainability for computerized tomography image segmentation," *Explainable AI in healthcare: Unboxing machine learning for biomedicine*, M. S. Raval, M. Roy, T. Kaya, and R. Kapdi, Eds.: Chapman and Hall/CRC, 2023. [Online]. Available: <https://doi.org/10.1201/9781003333425-5>
- [27] A. Bouhuys, *The Physiology of Breathing: A Textbook for Medical Students*. Grune & Stratton, 1977.
- [28] E. R. Weibel, *Morphometry of the Human Lung*. Springer, 1963.
- [29] A. A. Diaz *et al.*, "Airway Count and Emphysema Assessed by Chest CT Imaging Predicts Clinical Outcome in Smokers," *Chest*, vol. 138, no. 4, pp. 880-887, 2010/10/01/ 2010, doi: <https://doi.org/10.1378/chest.10-0542>.
- [30] S. E. Verleden *et al.*, "Small airways pathology in idiopathic pulmonary fibrosis: a retrospective cohort study," *Lancet Respir Med*, vol. 8, no. 6, pp. 573-584, Jun 2020, doi: 10.1016/S2213-2600(19)30356-X.
- [31] M. Abbas, "Automatic Segmentation of Bronchiectasis Affected Lungs Using UNETs on Lung Computed Tomography Imaging," *Thesis, MEng in Computer Science, UCL Computer Science, University College London*, 2020.